Fractional order control and simulation of wind energy systems with PMSG/full-power converter topology

R. Melício [a], V.M.F. Mendes [b], J.P.S. Catalão [a,*]

[a] *Department of Electromechanical Engineering, University of Beira Interior, R. Fonte do Lameiro, 6201-001 Covilha, Portugal*
[b] *Department of Electrical Engineering and Automation, Instituto Superior de Engenharia de Lisboa, R. Conselheiro Emídio Navarro, 1950-062 Lisbon, Portugal*

Received 25 May 2009

Abstract

This paper presents a new integrated model for the simulation of wind energy systems. The proposed model is more realistic and accurate, considering a variable-speed wind turbine, two-mass rotor, permanent magnet synchronous generator (PMSG), different power converter topologies, and filters. Additionally, a new control strategy is proposed for the variable-speed operation of wind turbines with PMSG/full-power converter topology, based on fractional-order controllers. Comprehensive simulation studies are carried out with matrix and multilevel power converter topologies, in order to adequately assert the system performance in what regards the quality of the energy injected into the electric grid. Finally, conclusions are duly drawn.

Keywords: Wind energy; modeling and simulation; permanent magnet synchronous generator; fractional-order control

1. Introduction

Wind energy is the fastest growing energy technology in terms of percentage of yearly growth of installed capacity per technology source [1].

In Portugal, the wind power goal foreseen for 2010 was established by the government as 3750 MW and that will constitute some 25% of the total installed capacity by 2010 [2]. This value has recently been raised to 5100 MW, by the most recent governmental goals for the wind sector. Hence, Portugal has one of the most ambitious goals in terms of wind power, and in 2006 was the second country in Europe with the highest wind power growth.

* Corresponding author. Tel.: +351 275 329914; fax: +351 275 329972.
E-mail address: catalao@ubi.pt (J.P.S. Catalão).

As wind energy is increasingly integrated into power systems, the stability of already existing power systems is becoming a concern of utmost importance [3]. Also, network operators have to ensure that consumer power quality is not deteriorated. Hence, the total harmonic distortion (THD) should be kept as low as possible, improving the quality of the energy injected into the electric grid [4]. The new technical challenges emerging due to increased wind power penetration, dynamic stability and power quality imply research of more realistic and accurate models for wind energy systems.

Power-electronic converters have been developed for integrating wind power with the electric grid. The use of power-electronic converters allows not only for variable-speed operation of a wind turbine, but also for enhancement on power extraction [5]. In a recent overview of different wind generator systems [6], it is shown that variable-speed conceptions equipped with power-electronic converts will continue to dominate and be very promising technologies for large wind farms.

Variable-speed control is better than constant-speed control and is known for at least a decade [7]. In a variable-speed wind turbine with full-power converter, the wind turbine is directly connected to the generator and the generator is completely decoupled from the electric grid. Of all the generators used in wind turbines, the permanent magnet synchronous generator (PMSG) is the one with a significant advantage: it is stable and secure under normal operating conditions; and comparing with a wound synchronous generator, it is smaller and does not need a direct current power source for field excitation.

Accurate modeling and control of wind turbines have high priority in the research activities all over the world [8]. Also, understanding the harmonic behavior of variable-speed wind turbines is essential in order to analyze their effect on the electric grids where they are connected [9]. At the moment, substantial documentation exists on modeling and control issues for the doubly fed induction generator (DFIG) wind turbine. But this is not the case for wind turbines with PMSG and full-power converter.

In this paper, a variable-speed wind turbine is considered with PMSG and different power converter topologies: matrix, and multilevel.

Matrix converters have received considerable attention during the past decades, since they may become a viable alternative to back-to-back converters [10]. The matrix converter is capable of converting the variable AC from the generator into constant AC to the electric grid in one stage. A technology review of matrix converters can be seen in [11]. The converter is smaller, lighter and more reliable than conventional converters, representing a good alternative for variable-speed operation of wind

energy systems [12]. One of the major drawbacks of a matrix converter is that 18 total switches are required, causing an increase in converter semiconductor cost. Also, industrial wide use of matrix converter is still very limited due to certain undesirable characteristics: its sensitivity to distortion in input power supply due to the lack of reactive component in the power circuit, and its sensitivity to the rapidly fluctuating input voltage frequency when used in wind energy systems [13].

Multilevel converters are widely used in high-voltage and high-power applications [14, 15], because they allow operations at higher dc-link voltage levels, avoiding the problems of the series interconnection of devices [16]. Compared to the conventional two-level converter topology, multilevel converters provide several advantages: their ability to meet the increasing demand of power ratings and power quality associated with reduced harmonic distortion, lower electromagnetic interference, and higher efficiencies [17]. Hence, multilevel converters are a good tradeoff solution between performance and cost in high-power systems [18]. A survey of topologies, controls, and applications for multilevel inverters can be seen in [19]. Multilevel converters are, however, limited by the following drawbacks: voltage unbalances, high component count, and increased control complexity. A critical issue in multilevel converters is the design of the DC-link capacitors. Thus, special attention should be paid to the unbalance in the capacitors' voltage of multilevel converters, which may produce a malfunction of the control. One possible design of the DC-link is given in [20].

Several papers have been issued on matrix and multilevel power converters, but mainly using simplified models to describe the wind energy system or the control strategies themselves. However, the increased wind power penetration, as nowadays occurs for instance in Portugal, requires new models for the simulation of wind energy systems, more realistic and accurate, and new control strategies, improving performance of disturbance attenuation and system robustness. These concerns are all accounted for in our paper.

As a new contribution to earlier studies, an integrated model for the simulation of wind energy systems with different power converter topologies is presented in this paper. Additionally, a new fractional-order control strategy is proposed for the variable-speed operation of wind turbines with PMSG/full-power converter topology.

Harmonic emissions are recognized as a power quality problem for modern variable-speed wind turbines. Understanding the harmonic behavior of variable-speed wind turbines is essential in order to analyze their effect on the electric grids where they are connected [9]. Hence, comprehensive simulation studies are carried out with matrix and multilevel power converter topologies, in order to adequately assert the system performance in what regards the quality of the energy injected into the electric grid.

This paper is organized as follows. Section 2 presents the integrated modeling of the wind energy system with different power converter topologies: matrix and multilevel. Section 3 presents the new fractional-order control strategy for the variable-speed operation of wind turbines with PMSG/full-power converter topology. Section 4 provides the power quality evaluation by Fast Fourier Transform (FFT) and THD. Section 5 presents the simulation results obtained on a case study. Finally, concluding remarks are given in Section 6.

2. Integrated modeling

The notation used throughout the paper is stated as follows.

P_t Mechanical power of the turbine.

ρ Air density.

A Area covered by the rotor.

R Radius of the area covered by the blades.

u Wind speed value upstream of the rotor.

c_p Power coefficient.

θ Pitch angle of the rotor blades.

λ Tip speed ratio.

ω_t Rotor angular speed at the wind turbine.

J_t Moment of inertia for blades and hub.

T_t Mechanical torque.

T_{dt} Resistant torque in the wind turbine bearing.

T_{at} Resistant torque in the hub and blades.

T_{ts} Torsional stiffness torque.

ω_g Rotor angular speed at the generator.

J_g Moment of inertia for the rotor of the generator.

T_{dg} Resistant torque in the generator bearing.

T_{ag} Resistant torque due to the viscosity of the airflow in the generator.

T_g Electric torque.

i_d , i_q Stator currents.

L_d , L_q Stator inductances.

u_d , u_q Stator voltages.

p Number of pairs of poles.

M Mutual inductance.

R_d , R_q Stator resistances.

i_f Equivalent rotor current.

2.1 Wind turbine

The mechanical power of the turbine is given by:

$$P_t = \frac{1}{2}\rho A u^3 c_p \tag{1}$$

The computation of the power coefficient requires the use of blade element theory and the knowledge of blade geometry. The power coefficient is a function of the pitch angle of rotor blades and the tip seed ratio, which is the ratio between blade tip speed and wind speed upstream of the rotor. In this paper, the numerical approximation developed in [21] is followed, where the power coefficient is given by:

$$c_p = 0.73\left(\frac{151}{\lambda_i} - 0.58\theta - 0.002\theta^{2.14} - 13.2\right)e^{-\frac{18.4}{\lambda_i}} \tag{2}$$

$$\lambda_i = \frac{1}{\frac{1}{(\lambda - 0.02\theta)} - \frac{0.003}{(\theta^3 + 1)}} \tag{3}$$

The mechanical power acquired from the wind is given by (1) to (3). From (2), the maximum power coefficient is given for a null pitch angle and it is equal to:

$$c_{p\max} = 0.4412 \tag{4}$$

corresponding to an optimal tip speed ratio equal to:

$$\lambda_{opt} = 7.057 \tag{5}$$

In order to achieve maximum power, the tip speed ratio should be kept at the value corresponding to the global maximum for the power coefficient [5]. Hence, the rotor angular speed at the wind turbine is as a function of the maximum mechanical power $P_{t\max}$, given by:

$$\omega_t = \lambda_{opt} \sqrt[3]{\frac{2\ P_{t\max}}{\rho\ \pi R^5 c_{p\max}}} \tag{6}$$

A maximum power point tracking (MPPT) is used in determining the optimal rotor angular speed at the wind turbine for each wind speed to obtain maximum rotor power [5].

When regulating the wind system under the specification of maximum power, it must be taken into account that turbine power must never be higher than generator value for the rated power. Once generator rated power is reached at rated wind speed it must be limited. For variable-speed wind turbines, a blade active pitch angle controller must be included [22], employing pitch control when reducing the angle of attack: increasing the blade pitch angle reduces the power coefficient and maintain the power at its rated value. When rated turbine speed is reached, control strategy must be changed so that a higher wind velocity no longer increases turbine speed but increases generated power until generator rated power; increases in rotor speed of about 10% are allowed during transients because of the slow pitch control response [23].

Fig. 1 shows the power coefficient as a function of the tip speed ratio, parameterized in function of the pitch angle.

"See Fig. 1 at the end of the manuscript".

2.2 Two-mass drive train model

An accurate way to model a mechanical drive train of a wind energy system is to model the rotor as a number of equivalent discrete masses connected together by springs and dampers. A two-mass model for the mechanical drive train is considered in this paper: one mass represents the blades and the hub joint, the wind turbine moment of inertia, and the other mass represents the generator moment of inertia. The configuration of the simulated mechanical drive train is shown in Fig. 2.

"See Fig. 2 at the end of the manuscript".

The equations for the two-mass model are based on the torsional version of the second law of Newton, deriving the state equation for the rotor angular speed at the wind turbine and for the rotor angular speed at the generator, respectively given by:

$$\frac{d\omega_t}{dt} = \frac{1}{J_t}\left(T_t - T_{dt} - T_{at} - T_{ts}\right) \tag{7}$$

$$\frac{d\omega_g}{dt} = \frac{1}{J_g}\left(T_{ts} - T_{dg} - T_{ag} - T_g\right) \tag{8}$$

2.3 Generator

The model for the PMSG is the usual one, where the state equations for modeling the PMSG stator currents, using motor machine convention, are given by:

$$\frac{di_d}{dt} = \frac{1}{L_d}\left[u_d + p\,\omega_g\,L_q\,i_q - R_d\,i_d\right] \tag{9}$$

$$\frac{di_q}{dt} = \frac{1}{L_q}\left[u_q - p\,\omega_g\left(L_d\,i_d + M\,i_f\right) - R_q\,i_q\right] \tag{10}$$

In order to avoid demagnetization of permanent magnet in the PMSG, a null stator current $i_d = 0$ is imposed [24]. The electric power is given by:

$$P_g = [u_d \quad u_q \quad u_f][i_d \quad i_q \quad i_f]^T \tag{11}$$

2.4 Matrix converter

The matrix converter is an AC-AC converter, with nine bidirectional commanded insulated gate bipolar transistors (IGBTs) S_{ij}. It is connected between a first order filter and a second order filter. The first order filter is connected to a PMSG, while the second order filter is connected to an electric network. A switching strategy can be chosen so that the output voltages have nearly sinusoidal waveforms at the desired frequency, magnitude and phase angle, and the input currents are nearly sinusoidal at the desired displacement power factor [25]. A three-phase active symmetrical circuit in series models the electric network. The phase currents injected in the electrical grid are modeled by the state equation using, given by:

$$\frac{di_{fj}}{dt} = \frac{1}{L_n}\left(u_{fj} - R_n\,i_{fj} - u_j\right) \qquad j = \{4,5,6\} \tag{12}$$

The configuration of the simulated wind energy system with matrix converter is shown in Fig. 3.

"See Fig. 3 at the end of the manuscript".

The IGBTs commands S_{ij} are given in function of the on and off states, as follows:

$$S_{ij} = \begin{cases} 1, & (\text{on}) \\ 0, & (\text{off}) \end{cases} \qquad i, j \in \{1, 2, 3\} \tag{13}$$

For the matrix converter modeling it is considered that:

$$\sum_{j=1}^{3} S_{ij} = 1 \qquad i \in \{1, 2, 3\} \tag{14}$$

$$\sum_{i=1}^{3} S_{ij} = 1 \qquad j \in \{1, 2, 3\} \tag{15}$$

The vector of output phase voltages is related to the vector of input phase voltages through the command matrix [26], as follows:

$$\begin{bmatrix} v_A \\ v_B \\ v_C \end{bmatrix} = \begin{bmatrix} S_{11} & S_{12} & S_{13} \\ S_{21} & S_{22} & S_{23} \\ S_{31} & S_{32} & S_{33} \end{bmatrix} \begin{bmatrix} v_a \\ v_b \\ v_c \end{bmatrix} = [S] \begin{bmatrix} v_a \\ v_b \\ v_c \end{bmatrix} \tag{16}$$

The vector of input phase currents is related to the vector of output phase currents through the command matrix [26], as follows:

$$[i_a \quad i_b \quad i_c]^T = [S]^T \, [i_A \quad i_B \quad i_C]^T \tag{17}$$

2.5 Multilevel converter

The multilevel converter is an AC/DC/AC converter, with twelve unidirectional commanded IGBTs S_{ij} used as a rectifier, and with the same number of unidirectional commanded IGBTs used as an inverter. A group of four IGBTs linked to the same phase constitute a leg j of the converter. The rectifier is connected between the PMSG and a capacitor bank. The inverter is connected between this capacitor bank and a second order filter, which in turn is connected to an electric grid. Again, a three-phase active symmetrical circuit in series models the electric grid [27, 28]. The phase currents injected in the electric grid are modeled by the state equation (12).

The configuration of the wind energy system with multilevel converter is shown in Fig. 4.

"See Fig. 4 at the end of the manuscript".

The switching variable γ_j of each leg j is a function of the states S_{ij} of the converter. The index i with $i \in \{1,2,3,4\}$ identifies the IGBT. The index j with $j \in \{1,2,3\}$ identifies the leg for the rectifier and $j \in \{4,5,6\}$ identifies the inverter one. The three valid conditions [29] for the switching variable of each leg j are given by:

$$\gamma_j = \begin{cases} 1, & (S_{1j} \text{ and } S_{2j}) = 1 \quad \text{and} \quad (S_{3j} \text{ or } S_{4j}) = 0 \\ 0, & (S_{2j} \text{ and } S_{3j}) = 1 \quad \text{and} \quad (S_{1j} \text{ or } S_{4j}) = 0 \\ -1, & (S_{3j} \text{ and } S_{4j}) = 1 \quad \text{and} \quad (S_{1j} \text{ or } S_{2j}) = 0 \end{cases} \qquad j \in \{1,\ldots,6\} \tag{18}$$

A switching variable Φ_{1j} is associated with the two upper IGBTs in each leg j (S_{1j} and S_{2j}), and also a switching variable Φ_{2j} is associated with the two lower IGBTs (S_{3j} and S_{4j}), respectively given by:

$$\Phi_{1j} = \frac{\gamma_j(1+\gamma_j)}{2} \;\; ; \;\; \Phi_{2j} = \frac{\gamma_j(1-\gamma_j)}{2} \qquad j \in \{1,\ldots,6\} \tag{19}$$

Hence, each switching variable depends only on the conducting and blocking states of the IGBTs. The voltage v_{dc} is the sum of the voltages v_{C1} and v_{C2} in the capacitor banks C_1 and C_2, modeled by the state equation, given by:

$$\frac{dv_{dc}}{dt} = \frac{1}{C_1}\left(\sum_{j=1}^{3}\Phi_{1j}i_j - \sum_{j=4}^{6}\Phi_{1j}i_j\right) + \frac{1}{C_2}\left(\sum_{j=1}^{3}\Phi_{2j}i_j - \sum_{j=4}^{6}\Phi_{2j}i_j\right) \tag{20}$$

3. Control strategy

3.1 Fractional-order controller

A novel control strategy based on fractional-order PI^{μ} controllers is proposed for the variable-speed operation of wind turbines with PMSG and full-power converters. Fractional calculus theory is a generalization of ordinary differentiation and integration to arbitrary (non-integer) order [30]. Recently, applications of fractional calculus theory in practical control field have increased significantly [31].

The fractional-order differentiator can be denoted by a general operator ${}_aD_t^{\mu}$ [32], given by:

$$ {}_aD_t^{\mu} = \begin{cases} \dfrac{d^{\mu}}{dt^{\mu}}, & \Re(\mu) > 0 \\ 1, & \Re(\mu) = 0 \\ \int_a^t (d\tau)^{-\mu}, & \Re(\mu) < 0 \end{cases} \tag{21} $$

where μ is the order of derivative or integrals, $\Re(\mu)$ is the real part of the μ. The mathematical definition of fractional derivatives and integrals has been the subject of several descriptions. The most frequently encountered one is called Riemann–Liouville definition, in which the fractional-order integral is given by:

$$ {}_aD_t^{-\mu} f(t) = \frac{1}{\Gamma(\mu)} \int_a^t (t-\tau)^{\mu-1} f(\tau)\, d\tau \tag{22} $$

while the definition of fractional-order derivatives is:

$$ {}_aD_t^{\mu} f(t) = \frac{1}{\Gamma(n-\mu)} \frac{d^n}{dt^n} \left[\int_a^t \frac{f(\tau)}{(t-\tau)^{\mu-n+1}}\, d\tau \right] \tag{23} $$

where:

$$ \Gamma(x) \equiv \int_0^{\infty} y^{x-1}\, e^{-y}\, dy \tag{24} $$

is the Euler's Gamma function, a and t are the limits of the operation, and μ is the number identifying the fractional order. In this paper, μ is assumed as a real number that satisfies the restrictions $0 < \mu \le 1$. Also, it is assumed that $a = 0$. The following convention is used: ${}_0D_t^{-\mu} \equiv D_t^{-\mu}$.

The other approach is Grünwald–Letnikov definition of fractional-order integral, given by:

$$ {}_aD_t^{-\mu} f(t) = \lim_{h \to 0} h^{\mu} \sum_{r=0}^{\frac{t-a}{h}} \frac{\Gamma(\mu + r)}{r!\,\Gamma(\mu)} f(t - r\,h) \tag{25} $$

while the definition of fractional-order derivatives is:

$$ {}_aD_t^{\mu} f(t) = \lim_{h \to 0} h^{-\mu} \sum_{r=0}^{\frac{t-a}{h}} (-1)^r \frac{\Gamma(\mu + 1)}{r!\,\Gamma(\mu - r + 1)} f(t - r\,h) \tag{26} $$

where the binomial coefficients $(r > 0)$ are given by: definition, given by:

$$ \binom{\mu}{0} = 1, \quad \binom{\mu}{r} = \frac{\mu(\mu-1)\ \ldots\ (\mu - r + 1)}{r!} \tag{27} $$

An important property revealed by (25) is that while integer-order operators imply finite series, the fractional-order counterparts are defined by infinite series. This means that integer operators are local operators in opposition with the fractional operators that have, implicitly, a memory of all past events.

The differential equation of the fractional-order PI^{μ} controller, $0 < \mu < 1$, in time domain, is given by:

$$u(t) = K_p\, e(t) + K_i\, D_t^{-\mu}\, e(t) \tag{28}$$

where K_p is a proportional constant and K_i is an integration constant. Taking $\mu = 1$ in (28), a classical PI controller is obtained. Hence, using Laplace transforms the transfer function of the fractional-order PI^{μ} and proportional integral PI controllers are respectively given by:

$$G(s) = K_p + K_i\, s^{-\mu} \tag{29}$$

$$G(s) = K_p + K_i\, s \tag{30}$$

3.2 Converters control

Power converters are variable structure systems, because of the on/off switching of their IGBTs. As mentioned previously, the controllers used in the converters are respectively proportional integral and fractional-order PI^{μ} controllers. Pulse width modulation (PWM) by space vector modulation (SVM) associated with sliding mode is used for controlling the converters.

The sliding mode control strategy presents attractive features such as robustness to parametric uncertainties of the wind turbine and the generator as well as to electric grid disturbances [33].

Sliding mode controllers are particularly interesting in systems with variable structure, such as switching power converters, guaranteeing the choice of the most appropriate space vectors. Their aim is to let the system slide along a predefined sliding surface by changing the system structure.

The power semiconductors present physical limitations that have to be considered during design phase and during simulation study. Particularly, they cannot switch at infinite frequency. Also, for a finite value of the switching frequency, an error $e_{\alpha\beta}$ will exist between the reference value and the control value. In order to guarantee that the system slides along the sliding surface $S(e_{\alpha\beta}, t)$, it has been proven that it is necessary to ensure that the state trajectory near the surfaces verifies the stability conditions [26] given by:

$$S(e_{\alpha\beta},t)\ \frac{dS(e_{\alpha\beta},t)}{dt}<0 \tag{31}$$

in practice a small error $\varepsilon>0$ for $S(e_{\alpha\beta},t)$ is allowed, due to power semiconductors switching only at finite frequency. Consequently, a switching strategy has to be considered, given by:

$$-\varepsilon < S(e_{\alpha\beta},t) < +\varepsilon \tag{32}$$

The output voltages of matrix converter are switched discontinuous variables. If high enough switching frequencies are considered (much higher than the input and output matrix converter fundamental frequencies), it is possible to assume that in each switching period T_s, the average value of the output voltages is nearly equal to their reference average value. Hence, the following equality is assumed:

$$\frac{1}{T_s}\int_{nT_s}^{(n+1)T_s} v_{\alpha\beta}\ dt = v_{\alpha\beta}^{*} \tag{33}$$

Similar to output voltages, the input current average value is nearly equal to their reference average value. Hence, the following equality is also assumed:

$$\frac{1}{T_s}\int_{nT_s}^{(n+1)T_s} i_q\ dt = i_q^{*} \tag{34}$$

The output voltage vectors and the input current vectors in the $\alpha\beta$ plane for the matrix converter are shown in Fig. 5 and Fig. 6, respectively.

"See Fig. 5 at the end of the manuscript".

"See Fig. 6 at the end of the manuscript".

The output voltage vectors in the $\alpha\beta$ plane for the multilevel converter are shown in Fig. 7.

"See Fig. 7 at the end of the manuscript".

4. Power quality assessment

The harmonic behavior computed by the FFT is based on Fourier analysis. If is $X(\omega)$ a continuous periodical signal with period of T and satisfies Dirichlet condition, the Fourier series is given by:

$$X(\omega)=\sum_{n=1}^{N} x(n)e^{-j\omega n} \quad \text{for } 0\le\omega\le 2\pi \tag{35}$$

In order to implement Fourier analysis in a computer, the signal in both time and frequency domains is discrete and has finite length with N points per cycle. Hence, Discrete Fourier Transform (DFT) is introduced, given by:

$$X(k) = \sum_{n=1}^{N} W^{(n-1)(k-1)} x(n) \text{ for } k = 1,2,..., N \tag{36}$$

where $x(n)$ is the Fourier coefficient at kth harmonic, $W = e^{(-j2\pi n/N)}$ is the spectrum of $x(n)$.

The harmonic behavior computed by the THD is given by:

$$\text{THD}\ (\%) = 100 \frac{\sqrt{\sum_{H=2}^{50} X_H^2}}{X_F} \tag{37}$$

where X_H is the root mean square (RMS) value of the signal, and X_F is the RMS value of the fundamental component.

5. Simulation results

The wind energy system considered has a rated electric power of 900 kW, and the time horizon considered in the simulation is 3.5 s. The mathematical models for the wind energy system with the matrix and multilevel converters were implemented in Matlab/Simulink. In this paper, $\mu = 0.7$ is assumed.

A ramp wind speed increase upstream of the rotor is considered in the simulation, taking 2 s between the speed 5 and 25 m/s, maintaining this speed during the rest of the time horizon, which is 3.5 s in our simulation. The switching frequency used in the simulation results is 5 kHz.

The mechanical power of the wind turbine, the electric power of the PMSG, and the difference between these two powers, i.e., the accelerating power, are shown in Fig. 8.

"See Fig. 8 at the end of the manuscript".

The harmonic behavior computed by the FFT for the mechanical power of the wind turbine is shown in Fig. 9.

"See Fig. 9 at the end of the manuscript".

The current injected in the electric grid with the matrix converter is shown in shown in Fig. 10. The output RMS current injected in the electric grid with the matrix converter is shown in Fig. 11. The harmonic behavior for the current injected in the electric grid with the matrix converter, computed by the FFT and the THD, is shown in Figs. 12 and 13, respectively.

"See Fig. 10 at the end of the manuscript".

"See Fig. 11 at the end of the manuscript".

"See Fig. 12 at the end of the manuscript".

"See Fig. 13 at the end of the manuscript".

The current injected in the electric grid with the multilevel converter is shown in shown in Fig. 14. The output RMS current injected in the electric grid with the multilevel converter is shown in Fig. 15. The harmonic behavior for the current injected in the electric grid with the multilevel converter, computed by the FFT and the THD, is shown in Figs. 16 and 17, respectively.

"See Fig. 14 at the end of the manuscript".

"See Fig. 15 at the end of the manuscript".

"See Fig. 16 at the end of the manuscript".

"See Fig. 17 at the end of the manuscript".

Table 1 summarizes an overall comparison between the matrix and multilevel converters, regarding the THD. The proposed wind energy system with the multilevel converter achieved the best performance. Nevertheless, due to the new fractional-order control strategy proposed in this paper, the current THD with either matrix or multilevel converter is lower than 5% limit imposed by IEEE-519 standard [34].

"See Table 1 at the end of the manuscript".

6. Conclusions

The increased wind power penetration leads to new technical challenges, dynamic stability and power quality. The contributions of this paper are twofold. A new integrated model for the simulation of wind energy systems, more realistic and accurate, is presented in this paper considering different power converter topologies. Additionally, a new fractional-order control strategy is proposed for the variable-speed operation of wind turbines with PMSG/full-power converter topology. The simulation results show

that the proposed fractional-order control strategy improves the performance of disturbance attenuation and system robustness. Hence, the current THD with either matrix or multilevel converter is lower than 5% limit imposed by IEEE-519 standard, which is used as a guideline for comparison purposes.

References

[1] Ahmed NA, Miyatake M, Al-Othman AK. Power fluctuations suppression of stand-alone hybrid generation combining solar photovoltaic/wind turbine and fuel cell systems. Energy Conv Manag 2008;49:2711–9.
[2] Estanqueiro A, Castro R, Flores P, Ricardo J, Pinto M, Rodrigues R, Peças Lopes J. How to prepare a power system for 15% wind energy penetration: the Portuguese case study. Wind Energy 2008;11:75–84.
[3] Ullah NR, Thiringer T. Variable speed wind turbines for power system stability enhancement. IEEE Trans Energy Convers 2007;22:52–60.
[4] Carrasco JM, Franquelo LG, Bialasiewicz JT, Galvan E, Guisado RCP, Prats AM, Leon JI, Moreno-Alfonso N. Power-electronic systems for the grid integration of renewable energy sources: A survey. IEEE Trans Ind Electron 2006;53:1002–16.
[5] Baroudi JA, Dinavahi V, Knight AM. A review of power converter topologies for wind generators. Renew Energy 2007;32:2369–85.
[6] Li H, Chen Z. Overview of different wind generator systems and their comparisons. IET Renew Power Gener 2008;2:123–38.
[7] Hong YY, Lu SD, Chiou CS. MPPT for PM wind generator using gradient approximation. Energy Conv Manag 2009;50:82–9.
[8] Hansen AD, Michalke G. Modelling and control of variable-speed multi-pole permanent magnet synchronous generator wind turbine. Wind Energy 2008;11:537–54.
[9] Tentzrakis ST, Papathanassiou SA. An investigation of the harmonic emissions of wind turbines. IEEE Trans Energy Convers 2007;22:150–8.
[10] Wheeler PW, Clare JC, Apap M, Bradley KJ. Harmonic loss due to operation of induction machines from matrix converters. IEEE Trans Ind Electron 2008;55:809–16.
[11] Wheeler PW, Rodríguez J, Clare JC, Empringham L, Weinstein A. Matrix converters: A technology review. IEEE Trans Ind Electron 2002;49:276–88.
[12] Cardenas R, Peña R, Wheeler P, Clare J. Reactive power capability of WECS based on matrix converter. Electron Lett 2008;44:674–6.
[13] Jia S, Wang X, Tseng KJ. Matrix converters for wind energy systems. Proceedings of 2nd IEEE Conf Ind Electron Appl 2007;488–94.
[14] Ceballos S, Pou J, Robles E, Gabiola I, Zaragoza J, Villate JL, Boroyevich D. Three-level converter topologies with switch breakdown fault-tolerance capability. IEEE Trans Ind Electron 2008;55:982–95.
[15] Barros JD, Silva JF. Optimal predictive control of three-phase NPC multilevel converter for power quality applications. IEEE Trans Ind Electron 2008;55;3670–81.
[16] Busquets-Monge S, Ortega JD, Bordonau J, Beristáin JA, Rocabert J. Closed-loop control of a three-phase neutral-point-clamped inverter using an optimized virtual-vector-based pulsewidth modulation. IEEE Trans Ind Electron 2008;55;2061–71.
[17] Portillo RC, Prats MM, Leon JI, Sanchez JA, Carrasco JM, Galvan E, Franquelo LG. Modeling strategy for back-to-back three-level converters applied to high-power wind turbines. IEEE Trans Ind Electron 2006;53;1483–91.
[18] Alepuz S, Busquets-Monge S, Bordonau J, Gago J, Gonzalez D, Balcells J. Interfacing renewable energy sources to the utility grid using a three-level inverter. IEEE Trans Ind Electron 2006;53;1504–11.

[19] Rodriguez J, Lai J-S, Peng FZ. Multilevel inverters: A survey of topologies, controls, and applications. IEEE Trans Ind Electron 2002;49;724–38.
[20] Eloy-Garcia J, Arnaltes S, Rodriguez-Amenedo JL. Extended direct power control for multilevel inverters including DC link middle point voltage control. IET Electr Power Appl 2007;1;571–80.
[21] Slootweg JG, de Haan SWH, Polinder H, Kling WL. General model for representing variable speed wind turbines in power system dynamics simulations. IEEE Trans. Power Syst. 2003;28:144–51.
[22] Conroy JF, Watson R. Low-voltage ride-through of a full converter wind turbine with permanent magnet generator. IET Renew Power Gener 2007;1:182–9.
[23] Chinchilla M, Arnaltes S, Burgos JC. Control of permanent-magnet generators applied to variable-speed wind energy systems connected to the grid. IEEE Trans Energy Convers 2006;21:130–5.
[24] Senjyu T, Tamaki S, Urasaki N, Uezato K. Wind velocity and position sensorless operation for PMSG wind generator. Proceedings of 5th PEDC, 2003;787–92.
[25] Barakati SM, Aplevich JD, Kazerani M. Controller design for a wind turbine system including a matrix converter. Proceedings 2007 IEEE PES GM, 2007.
[26] Pinto S, Silva J. Sliding mode direct control of matrix converters. IET Electr Power Appl 2007;1:439–48.
[27] Melício R, Mendes VMF, Catalão JPS. Two-level and multilevel converters for wind energy systems: a comparative study. Proceedings of the 13th EPE-PEMC, 2008;1682–7.
[28] Melício R, Mendes VMF, Catalão JPS. Evaluating power quality in wind power generation systems with two-level and multi-level converters. Proceedings of the 6th MedPower Conf., 2008.
[29] Barros JD, Silva JF. Optimal predictive control of three-phase NPC multilevel converter for power quality applications. IEEE Trans Ind Electron 2008;55;3670–81.
[30] Podlubny I. Fractional-order systems and PI-lambda-D-mu-controllers. IEEE Trans Autom Control 1999;44:208–214.
[31] Li W, Hori Y, Peng FZ. Vibration suppression using single neuron-based PI fuzzy controller and fractional-order disturbance observer. IEEE Trans Ind Electron 2007;54;117–26.
[32] Calderón AJ, Vinagre BM, Feliu V. Fractional order control strategies for power electronic buck converters. Signal Processing 2006;86:2803–19.
[33] Beltran B, Ahmed-Ali T, Benbouzid MEH. Sliding mode power control of variable-speed wind energy conversion systems. IEEE Trans Energy Convers 2008;23:551–8.
[34] IEEE Guide for Harmonic Control and Reactive Compensation of Static Power Converters, IEEE Standard 519-1992.

Figure captions

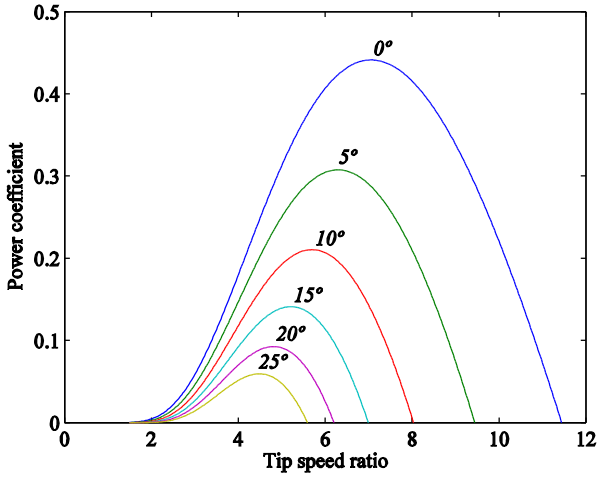

Fig. 1. Power coefficient as a function of the tip speed ratio, parameterized in function of the pitch angle.

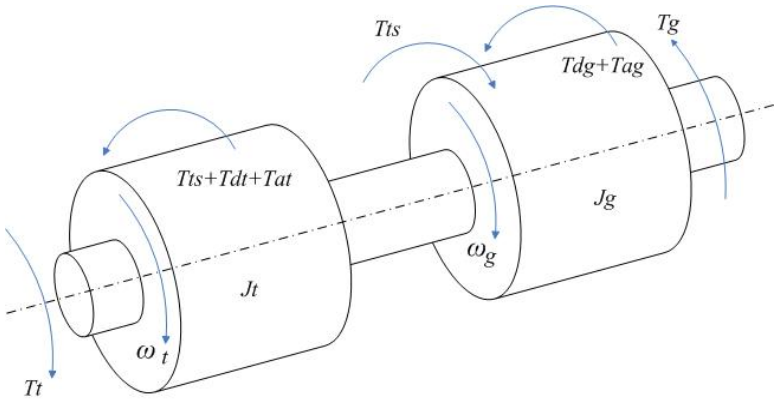

Fig. 2. Configuration of the two-mass drive train model.

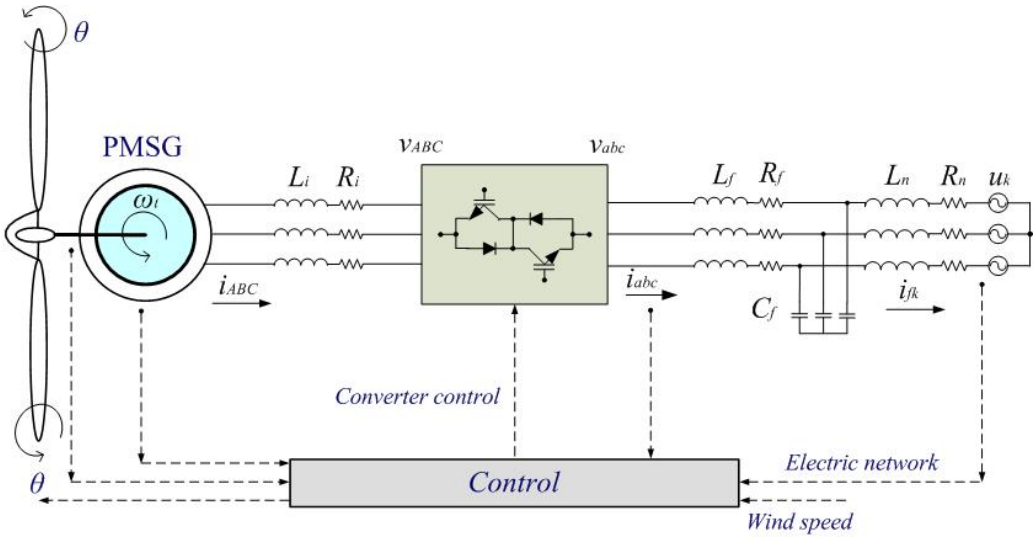

Fig. 3. Wind energy system with matrix converter.

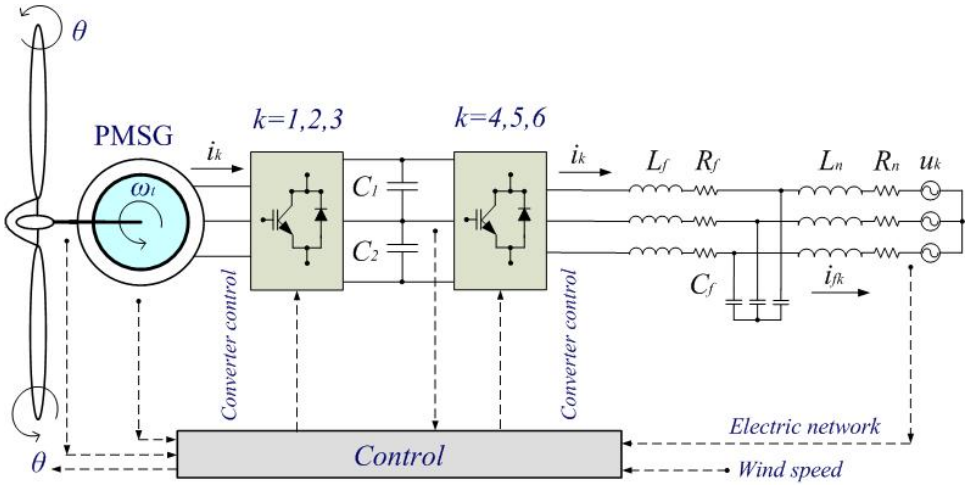

Fig. 4. Wind energy system with multilevel converter.

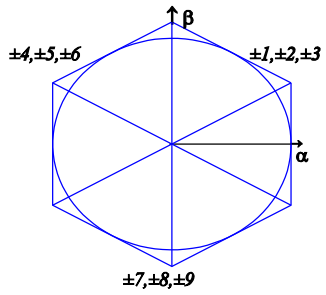

Fig. 5. Output voltage vectors for the matrix converter.

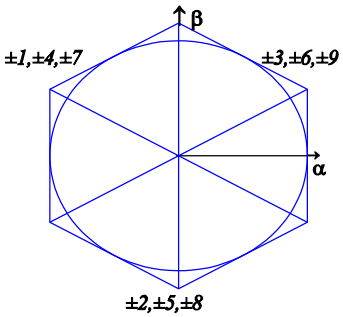

Fig. 6. Input current vectors for the matrix converter.

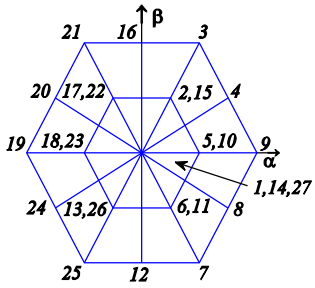

Fig. 7. Output voltage vectors for the multilevel converter.

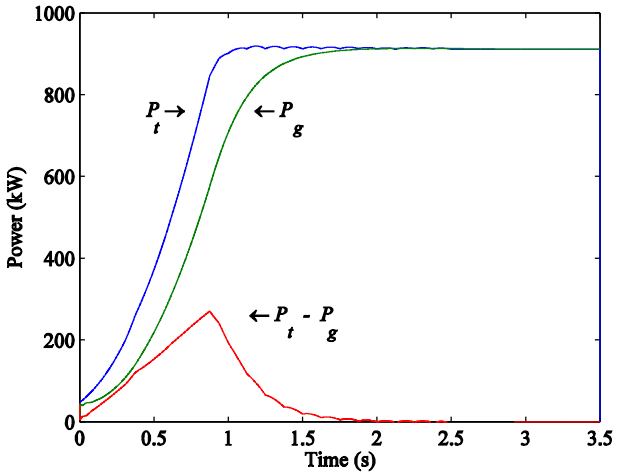

Fig. 8. Mechanical, electric and accelerating power.

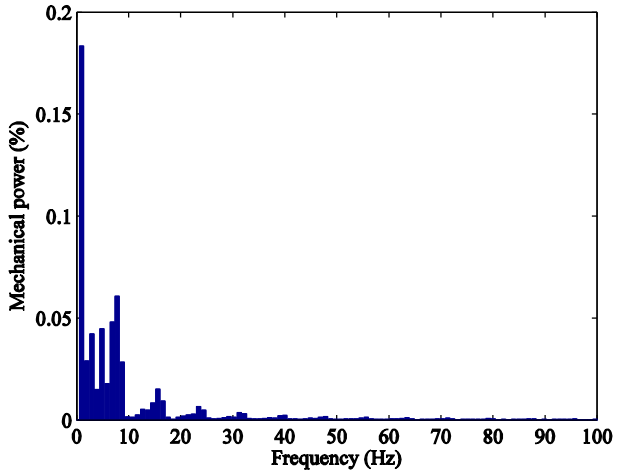

Fig. 9. Harmonic behavior for the mechanical power of the wind turbine.

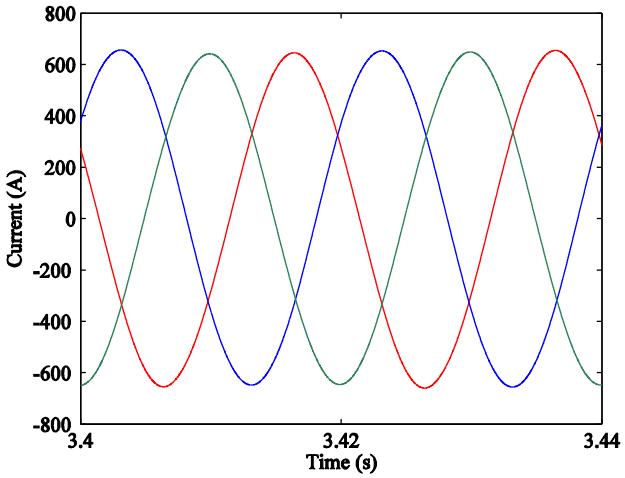

Fig. 10. Output current for the matrix converter.

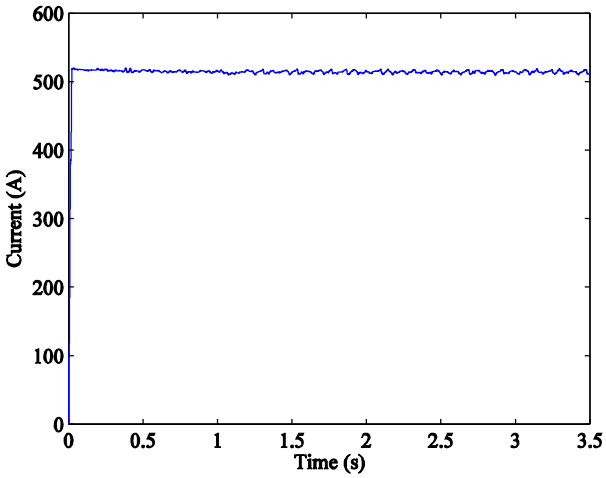

Fig. 11. Output RMS current for the matrix converter.

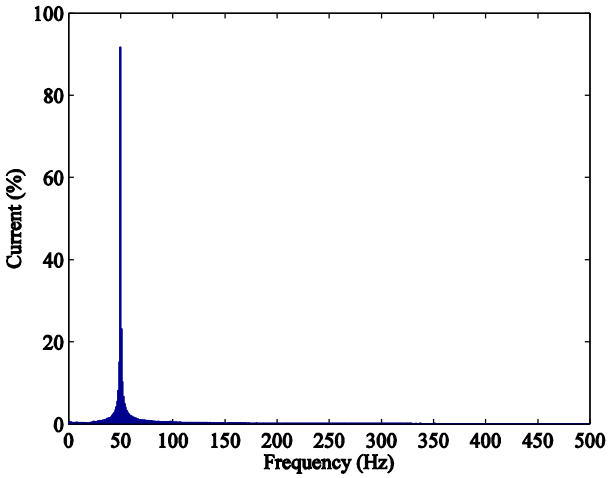

Fig. 12. FFT of the current injected in the grid with the matrix converter.

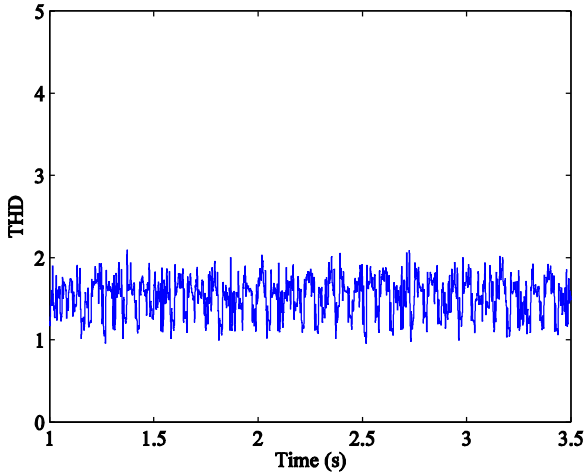

Fig. 13. THD of the current injected in the grid with the matrix converter.

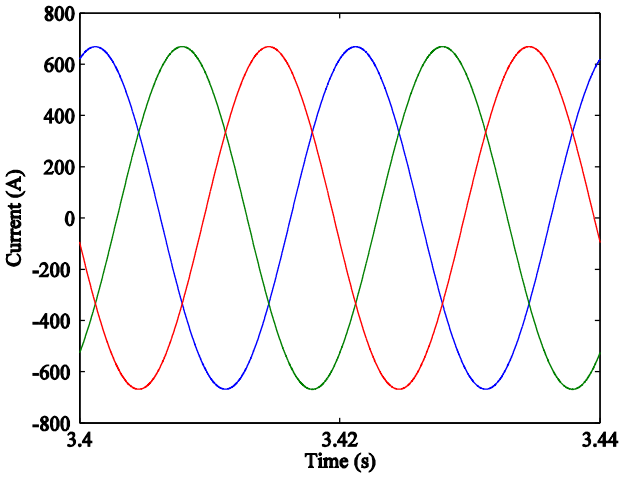

Fig. 14. Output current for the multilevel converter.

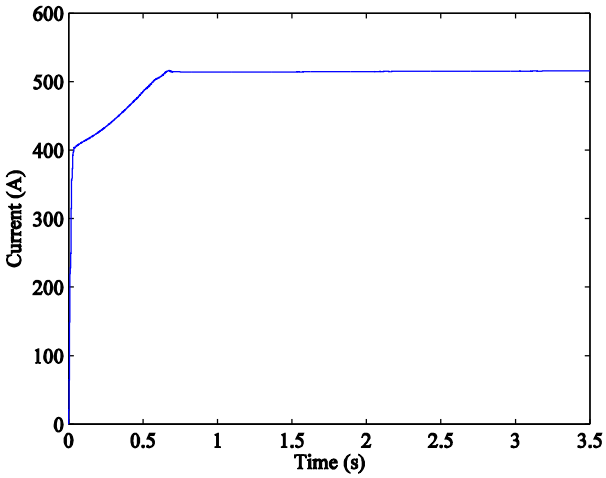

Fig. 15. Output RMS current for the multilevel converter.

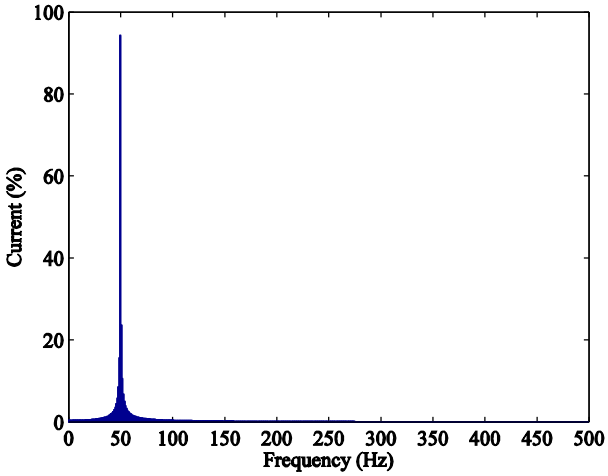

Fig. 16. FFT of the current injected in the grid with the multilevel converter.

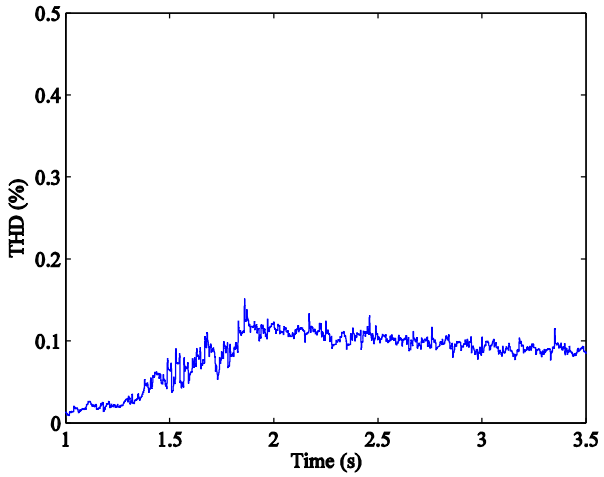

Fig. 17. THD of the current injected in the grid with the multilevel converter.

Tables

Table 1

THD of the current injected in the grid

Power converter topology	THD (%)
Matrix	2.13
Multilevel	0.10